Substrate-induced Conformational Changes in the Membrane-embedded IICmtl-domain of the Mannitol Permease from Escherichia coli, EnzymeIImtl, Probed by Tryptophan Phosphorescence Spectroscopy

Veldhuis, Gertjan; Gabellieri, Edi; Poolman, Bert; Strambini, Giovanni B.; Broos, Jaap

Published in:
The Journal of Biological Chemistry

DOI:
10.1074/jbc.M507061200

Publication date:
2005

THE JOURNAL OF BIOLOGICAL CHEMISTRY VOL. 280, NO. 42, pp. 35148–35156, October 21, 2005

Substrate-induced Conformational Changes in the Membrane-embedded IIC^{mtl}-domain of the Mannitol Permease from *Escherichia coli*, EnzymeII^{mtl}, Probed by Tryptophan Phosphorescence Spectroscopy*

Received for publication, June 28, 2005, and in revised form, August 4, 2005 Published, JBC Papers in Press, August 10, 2005, DOI 10.1074/jbc.M507061200

Gertjan Veldhuis[‡1], **Edi Gabellieri**[§], **Erwin P. P. Vos**[‡], **Bert Poolman**[‡], **Giovanni B. Strambini**[§2], **and Jaap Broos**[‡3]

From the [‡]*Department of Biochemistry and Biophysical Chemistry, Groningen Biomolecular Science and Biotechnology Institute, University of Groningen, Nijenborgh 4, 9747 AG Groningen, The Netherlands and the* [§]*Istituto di Biofisica, Consiglio Nazionale delle Ricerche, Area della Ricerca, Via Moruzzi 1, 56124 Pisa, Italy*

Membrane-bound transport proteins are expected to proceed via different conformational states during the translocation of a solute across the membrane. Tryptophan phosphorescence spectroscopy is one of the most sensitive methods used for detecting conformational changes in proteins. We employed this technique to study substrate-induced conformational changes in the mannitol permease, EnzymeII^{mtl}, of the phosphoenolpyruvate-dependent phosphotransferase system from *Escherichia coli*. Ten mutants containing a single tryptophan were engineered in the membrane-embedded IIC^{mtl}-domain, harboring the mannitol translocation pathway. The mutants were characterized with respect to steady-state and time-resolved phosphorescence, yielding detailed, site-specific information of the Trp microenvironment and protein conformational homogeneity. The study revealed that the Trp environments vary from apolar, unstructured, and flexible sites to buried, highly homogeneous, rigid peptide cores. The most remarkable example of the latter was observed for position 97, because its long sub-second phosphorescence lifetime and highly structured spectra in both glassy and fluid media imply a well defined and rigid core around the probe that is typical of β-sheet-rich structural motifs. The addition of mannitol had a large impact on most of the Trp positions studied. In the case of position 97, mannitol binding induced partial unfolding of the rigid protein core. On the contrary, for residue positions 126, 133, and 147, both steady-state and time-resolved data showed that mannitol binding induces a more ordered and homogeneous structure around these residues. The observations are discussed in context of the current mechanistic and structural model of EII^{mtl}.

The mannitol permease from the Gram-negative bacterium *Escherichia coli*, EnzymeII^{mtl} (EII^{mtl})[4,5] (1, 2), is responsible for the uptake and consecutive phosphorylation of mannitol (reviewed in Ref. 1). EII^{mtl} consists of three covalently linked domains (from N to C termini): a membrane-embedded IIC^{mtl}-domain harboring the mannitol-translocation pathway (2), and two cytosolic domains (IIB^{mtl} and IIA^{mtl}) responsible for phosphoryl transfer. EII^{mtl} becomes phosphorylated via a cascade of phosphoryl group-transfer reactions, starting with the hydrolysis of phosphoenolpyruvate by the cytosolic kinase EnzymeI (EI). The phosphate moiety from phosphorylated EI is transferred to HPr, a small cytosolic protein. Subsequently, His-554 in the IIA^{mtl}-domain is phosphorylated by P-HPr, and transfers the phosphate to Cys-384 in the IIB^{mtl}-domain. The phosphate is then donated to mannitol bound at the IIC^{mtl}-domain, resulting in the release of mannitol 1-phosphate in the cytoplasm. Phosphorylation of EII^{mtl} activates the carrier, resulting in a two-to-three orders of magnitude increase in the transport rate (3–5).

A *phoA* fusion study and hydropathy analysis of the IIC^{mtl}-domain resulted in a topology model with three small periplasmic loops, two large cytoplasmic loops, and six putative membrane-spanning helices (6). It has been proposed that both large cytoplasmic loops fold back into the membrane-embedded part of the protein, lining up a hydrophilic pathway for the translocation of the carbohydrate (7). New structural insight on the basis of cysteine-scanning mutagenesis in the first proposed cytoplasmic loop provided evidence for the presence of this loop protruding, at least partly, into the bilayer (8). For the subcloned IIC^{mtl}-domain, a two-dimensional projection structure at 5-Å resolution was determined by electron microscopy crystallography (9). Six regions of high density were found, possibly reflecting six membrane-spanning helices.

Of the available spectroscopic techniques, Trp phosphorescence spectroscopy is one of the most sensitive approaches used to study changes in protein conformation, due to the extremely slow (radiative) de-excitation rate of the triplet excited state (~0.2 s^{-1}). This makes Trp phosphorescence 10^8 times more sensitive for quenching processes than Trp fluorescence. A conformational change, nearby or more remote from the Trp probe, is expected to induce a different quenching pattern on this time scale, and thus a change in the phosphorescence lifetime (τ_P). The observation of multiple τ_P values for a single Trp position reflects the presence of different protein conformational states, which do not rapidly interchange on the time scale of τ_P. The ability to quench the Trp triplet state is governed by the local viscosity (η), and the relation between τ_P and η is well established (10, 11). The information obtained by measuring τ_P, combined with the recording of emission

* This work was supported in part by the Netherlands Organization of Scientific Research (NWO-CW) (Grant JC 99-535) and the Italian National Research Council. The costs of publication of this article were defrayed in part by the payment of page charges. This article must therefore be hereby marked "*advertisement*" in accordance with 18 U.S.C. Section 1734 solely to indicate this fact.

[1] Received a Netherlands Organization of Scientific Research (NWO-CW) travel grant.

[2] To whom correspondence may be addressed. Tel.: 39-050-315-3046; Fax: 39-050-315-2760; E-mail: giovanni.strambini@ib.pi.cnr.it.

[3] To whom correspondence may be addressed. Tel.: 31-(0)50–363-4277; Fax: 31-(0)50–363-4800; E-mail: j.broos@rug.nl.

[4] The abbreviations used are: EII^{mtl}, EnzymeII^{mtl} from *E. coli*; $\lambda_{0,0}$, peak wavelength of the 0,0-vibrational band in the phosphorescence spectrum; BW, bandwidth of the 0,0-vibrational band at 2/3-height; λ_g, centre of gravity of the phosphorescence spectrum; $\Delta\lambda_g(T)$, change in the centre of gravity upon thermal relaxation; τ_P, phosphorescence lifetime; λ_F, fluorescence emission maximum; mtl, mannitol; PG, 1,2-propyleneglycol; $C_{10}E_5$, decylpentaethyleneglycol ether; decylPEG, decylpoly(ethyleneglycol)300.

[5] Nomenclature of the enzymes: EII^{mtl}, wild-type EnzymeII^{mtl}; TL, EII^{mtl} where the four native tryptophans of wild-type EII^{mtl} (at positions 30, 42, 109, and 117) have been replaced with phenylalanines; Trp-66, Trp-97, Trp-114, Trp-126, Trp-133, Trp-147, Trp-167, Trp-188, and Trp-198 refer to single-Trp EII mutants based on TL; IIC-TL and IIC-Trp-97 refer to the subcloned IIC^{mtl}-domain of TL and Trp-97, respectively.

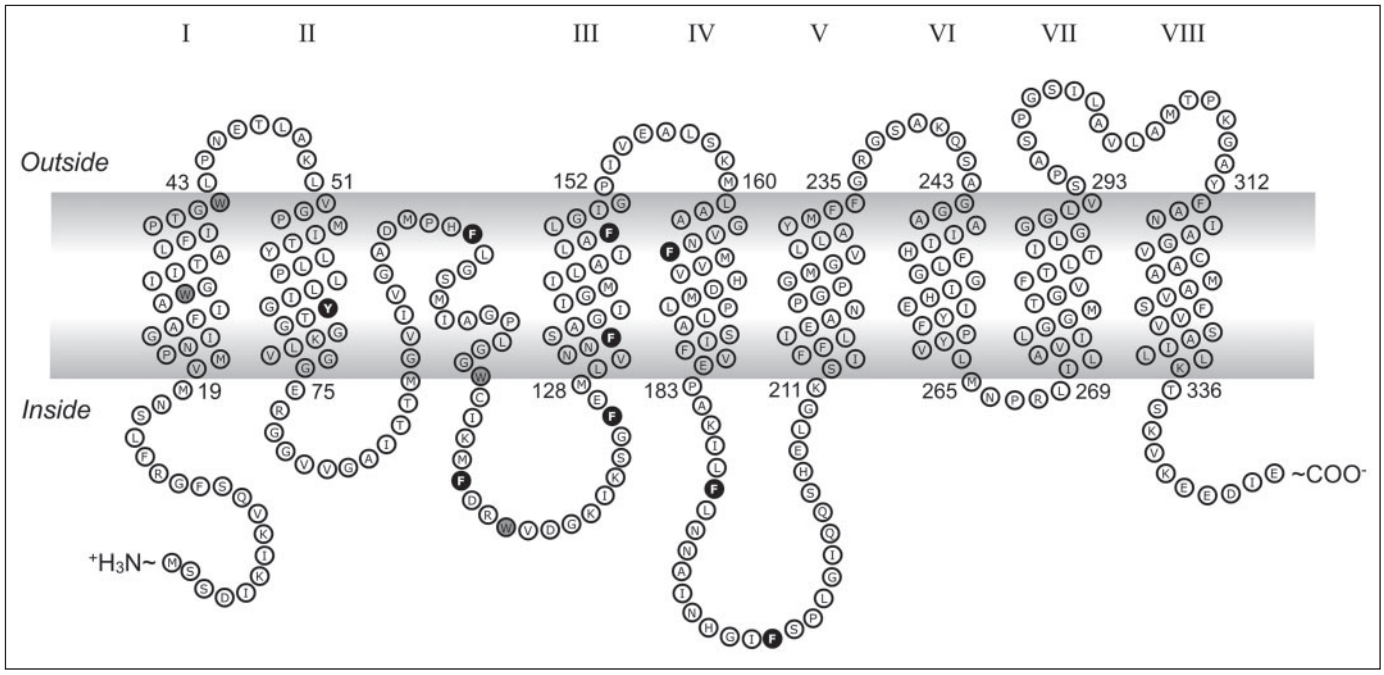

FIGURE 1. **Membrane topology model of the IIC^{mtl}-domain of EII^{mtl}.** The topology is based on the model presented by Vervoort *et al.* (8), using the algorithm TMHMM 2.0 (40) to determine the start and ending of transmembrane α-helices. *Outside* and *Inside* represent the peri- and cytoplasmic side of the membrane, respectively. The *Greek capitals* indicate the eight predicted transmembrane helices. The amino acid residues mutated into a tryptophan and used in this study are shown in *black*; the native tryptophans in the wild-type protein are shown in *gray*.

spectra of the protein in both the glass-state and in the fluid state, provides site-specific, structural information about the Trp microviscosity (η), micropolarity, and protein conformational heterogeneity. Together with fluorescence, phosphorescence can distinguish whether a residue is placed in a superficial, mobile, and solvent-exposed location in the protein or when it is in a buried and rigid part.

The wild-type EII^{mtl} protein has four Trp residues all located in the membrane-embedded IIC^{mtl}-domain. The fluorescence and phosphorescence characteristics of single-Trp mutants have pointed toward a large variation in polypeptide structure among the sites 30, 42, 109, and 117, as well a distinct response to the binding of mannitol and phosphorylation (12–16). The present study extends this approach with ten single-Trp mutants, containing tryptophans in either putative transmembrane helices or cytoplasmic loops of the IIC^{mtl}-domain (Fig. 1). The mutants were based on the functional Trp-less (TL) EII^{mtl} construct (12), in each case replacing an aromatic residue with a Trp between residues 66 and 198, encompassing the first half of the IIC^{mtl}-domain. The positions in the proposed topology model are helix II (Trp-66), a loop protruding the membrane (Trp-97), the following cytoplasmic loop (Trp-114 and Trp-126), helix III (Trp-133 and Trp-147), helix IV (Trp-167), and the following loop (Trp-188 and Trp-198).

Prominent among the findings reported here is the presence of an unexpectedly rigid, presumably β-sheet-rich segment in the loop between helices II and III, protruding into the lipid bilayer. More surprisingly, this structural part becomes largely unfolded upon binding of the substrate mannitol. There appeared to be no influence of the IIBA^{mtl}-domain on the structural characteristics of this part of the protein, as inferred from observations with IIC-Trp-97, lacking the cytoplasmic domains. Furthermore, the region from residues 125 to 150 becomes more structured upon mannitol binding.

MATERIALS AND METHODS

Chemicals and Reagents—D-[1-^{3}H]Mannitol (17.0 Ci/mmol, batch 3499-326) was purchased from PerkinElmer Life Sciences. D-[1-^{14}C]Mannitol (59.0 mCi/mmol, batch 78) was purchased from Amersham Biosciences. Radioactivity measurements were performed using Emulsifier Scintillator Plus obtained from Packard (Groningen, The Netherlands). Q-Sepharose and SP-Sepharose Fast Flow were from Amersham Biosciences. Ni-NTA resin was from Qiagen Inc. L-Histidine (spectroscopic grade) and imidazole were from Fluka. NaCl (Suprapure) was from Merck, Darmstadt, Germany. For phosphorescence measurements, water, doubly distilled over quartz, was purified by the Milli-Q Plus system (Millipore Corp., Bedford, MA). Spectroscopic grade 1,2-propylene glycol (PG) was from Merck. Decylpoly(ethylene glycol) 300 (decylPEG) was obtained from Kwant High Vacuum Oil Recycling and Synthesis, Bedum, The Netherlands. $C_{10}E_5$ (decyl pentaethylene glycol ether) was synthesized and purified as described previously (12). *n*-Decyl-β-D-maltopyranoside, Anagrade, was from Anatrace. All other chemicals were of the highest purity grade available from commercial sources. His-tagged versions of EI and HPr were created using standard genetic tools as will be described elsewhere.

Construction of Single-Trp Mutants—The construction of the functional Trp-less EII^{mtl} (TL) construct with a N-terminal His_6 tag will be published elsewhere.[6] In this construct all four native Trp residues at positions 30, 42, 109, and 117 were replaced with phenylalanines. The mutations resulting in the single-Trp mutants using TL as a basis (Trp-66, Trp-97, Trp-114, Trp-126, Trp-133, Trp-147, Trp-167, Trp-188, and Trp-198) were introduced using the QuikChange site-directed mutagenesis kit from Stratagene. In each mutant a phenylalanine was replaced with a Trp, except for Trp-66, where a tyrosine was mutated into a Trp. The sequences were confirmed by nucleotide sequence analysis. The IIC^{mtl} mutants were constructed by cutting the plasmids harboring the wild-type IIC^{mtl}-His_6 (with a C-terminal His_6 tag) (17), and TL and Trp-97 (EII constructs; see above), with restriction enzymes BbvC1 and Eco47III (at amino acid positions 15 and 237, respectively).

[6] E. P. P. Vos, manuscript in preparation.

The 665-bp fragment was isolated from the TL and Trp-97 mutants and ligated into the wild-type IIC^{mtl}-His$_6$ plasmid, without this 665-bp fragment, yielding IIC-Trp-97, and IIC-TL, respectively.

Cell Growth, Isolation of Inside-out Membrane Vesicles, and Protein Purification—The plasmids harboring the single-Trp-mutated *mtlA* genes (pMamtlaP_rHis$_6$EIItl-F→W or pMamtlaP_rIICtl-F→W-His$_6$) were transformed and subsequently grown in bacterial strain *E. coli* LGS322 (*F*$^-$ *thi-1*, *hisG1*, *argG6*, *metB1*, *tonA2*, *supE44*, *rspL104*, *lacY1*, *galT6*, *gatR49*, *gatA50*, Δ(*mtlA′p*), *mtlD*^{c}, Δ(*gutR′MDBA-recA*)) as described before (18). Inside-out membrane vesicles were prepared by passage of the cells through a French Press at 10.000 p.s.i., essentially as described (19). The membrane vesicles were washed once in 25 mM Tris-HCl, pH 7.6, 5 mM dithiothreitol, plus 1 mM NaN_3, and quickly frozen in small aliquots in liquid nitrogen prior to storage at −80 °C. Membrane vesicles used for experiments were placed at 37 °C for quick thawing and directly placed on ice until further used.

All single-Trp EII^{mtl} mutants were purified using Ni-NTA affinity chromatography as described (20). To remove all traces of the tryptophan phosphorescence quencher histidine (used to elute the protein from Ni-NTA) from the EII^{mtl} mutant preparations, pooled Ni-NTA fractions were diluted 5 times in buffer (25 mM Tris-HCl, pH 7.6, 2 mM reduced glutathione, plus 0.25% $C_{10}E_5$), loaded onto Q-Sepharose, washed with 20 column volumes of the same buffer, and subsequently eluted in a single step using 4 column volumes of the above buffer, supplemented with 400 mM NaCl (Suprapur, Merck). All fluorescence and phosphorescence measurements were performed using this buffer.

The Trp-less IIC-TL and single-Trp IIC-Trp-97 mutants were purified using a somewhat different strategy. Briefly, membrane vesicles (of ~20 mg/ml total membrane protein), harboring the overproduced IIC mutants, were solubilized at ~2 mg/ml in 25 mM Tris-HCl, pH 7.6, 400 mM NaCl, 10 mM 2-mercaptoethanol, 1% (w/v) *n*-decyl-β-D-maltopyranoside, plus 10 mM imidazole for 15 min at room temperature. After spinning down the non-solubilized material (10 min, 250,000 × *g*, 4 °C), the supernatant was mixed with washed Ni-NTA resin by stirring for 1 h at 4 °C. After draining the flow-through, the column was subsequently washed with 10 column volumes buffer A (25 mM Tris-HCl, pH 7.6, 200 mM NaCl, 0.35% decylPEG, 10 mM 2-mercaptoethanol, plus 10 mM imidazole), and 10 column volumes buffer B (25 mM Tris-HCl, pH 7.6, 150 mM NaCl, 0.25% decylPEG, plus 10 mM 2-mercaptoethanol). The His-tagged IIC^{mtl} mutants were batch-wise eluted from Ni-NTA with 80 mM L-histidine (in 25 mM Tris-HCl, pH 7.6, 150 mM NaCl, 0.25% decylPEG, plus 10 mM 2-mercaptoethanol). To remove the histidine, the same purification procedure as for the single-tryptophan EII^{mtl} mutants was followed, using SP-Sepharose instead of Q-Sepharose.

For both the EII^{mtl}- and IIC^{mtl} mutants, purification resulted in suitable protein samples for phosphorescence spectroscopy, typically at protein concentrations ranging from 5–15 μM. Protein purity of the samples was confirmed with SDS-PAGE analysis, and estimated to be >95%.

Mannitol Binding and Phosphorylation—Mannitol binding to detergent-solubilized membrane proteins was performed as described (21). The non-vectorial phosphoenolpyruvate-dependent phosphorylation activity of EII^{mtl} was measured as described (22). Briefly, the assay mixture contained 25 mM Tris-HCl, pH 7.6, 5 mM dithiothreitol, 5 mM $MgCl_2$, 5 mM phosphoenolpyrurate, 350 nM EI, 17 μM HPr, with or without 0.25% decylPEG, and rate-limiting amounts of EII^{mtl} (nanomolar regime). After incubation of the mixture for 5 min at 30 °C, the reaction was started by adding 1 mM [^{14}C]mannitol. The reaction was quenched at given time intervals by loading the samples on Dowex AG1-X2 columns (1 ml of resin). After washing the column with 4 column volumes of H_2O, formed [^{14}C]mannitol-1-phosphate was eluted using 2 column volumes of 0.2 N HCl and quantified by liquid scintillation counting.

Fluorescence Spectroscopy—For the purification of EII^{mtl} and IIC^{mtl}, care was taken to minimize fluorescent impurities in all used buffers (23). Steady-state measurements were performed on a Fluorolog3-22 spectrofluorometer (Jovin Yvon) at 20 °C. Excitation was at 295 nm with an excitation slit width of 2 nm and an emission slit width of 5 nm. All spectra were corrected for background fluorescence of the used buffers and instrument response. The changes in fluorescence after addition of 1 mM mannitol were calculated by integration of the spectra from 305–399 nm.

Phosphorescence Spectroscopy—For phosphorescence measurements in fluid solutions, O_2 removal was achieved by the alternative application of moderate vacuum and inlet of ultrapure N_2 (24). The samples were placed in specially designed T-shaped spectrosil quartz cuvettes (4-mm inner diameter round tubing in the optical section, Hellma, Mullheim/Baden, Germany) and rocked very gently, because of the surfactant, for about 10 min to achieve complete exchange of O_2 for N_2. The cuvette was connected to the N_2/vacuum line by peek tubing (1/16 inch), and the sample was fully isolated from the atmosphere by a septum (Hamilton 76003, Alltech, Lancashire, UK) plus O-ring seal assembly (24). Based on the phosphorescence lifetime of the protein alcohol dehydrogenase from horse liver, which exhibits one of the highest sensitivities to O_2 quenching, this procedure lowered the O_2 level <2 nM.

Phosphorescence spectra and decays were both measured with pulsed excitation (λ_{ex} = 288 nm) on a customized apparatus (24), modified to implement spectral measurements by means of a charge-coupled device camera. Pulsed excitation was provided by a frequency-doubled Nd/Yag-pumped dye laser (Quanta Systems, Milan, Italy) with pulse duration of 5 ns and a typical energy per pulse of 0.5–1 mJ. For spectra measurements the emission was collected at 90° from the excitation and dispersed by a 0.3-m focal length triple grating imaging spectrograph (SpectraPro-2300i, Acton Research Corp., Acton, MA) with a band pass ranging from 1.0 to 0.2 nm. The emission was monitored by a back-illuminated 1340- × 400-pixels charge-coupled device camera (Princeton Instruments, Spec-10:400B(XTE), Roper Scientific Inc., Trenton, NJ) cooled to −60 °C. In low temperature glasses, the phosphorescence spectrum of Trp was overlapped by a relatively intense background from solvent impurities and tyrosinate, an emission that decayed to negligible levels during the initial 3–4 s from the excitation pulse. Background-free Trp spectra were obtained by opening the mechanical shutter controlling the emission to the spectrograph after a delay of 3 s. In fluid solutions, where the lifetime of Trp phosphorescence is much shorter than the 6 s in glassy media, spectra were recorded by integrating multiple excitation pulses at a repetition frequency up to 10 Hz. To block overlapping prompt fluorescence and short-lived background from the detector, laser excitation was synchronized to a fast mechanical chopper opening the emission slit 35 μs after the laser pulse. In general, even with the shortest-lived protein phosphorescence less than 100 pulses was sufficient to obtain satisfactory signal-to-noise ratios. Besides averaging multiple pulses, the signal-to-noise ratio of very weak signals, which are characterized by relatively broad spectra, was further improved by horizontal binning of channels (2–4 channels), with no effect on spectral resolution. Under these extreme conditions the background signal, represented by a broad band peaked around 500 nm, was not negligible and was subtracted from the total spectrum, by using the spectrum of a TL control.

Phosphorescence decays were monitored by collecting the emission at 90° from vertical excitation through a filter combination with a trans-

TABLE ONE

Mannitol binding properties of the single-tryptophan mutants

Mutant	K_D[a]
	*n*M
EII^{mtl}-TL	70
Trp-66	141
Trp-97	1950
Trp-114	59
Trp-126	105
Trp-133	64
Trp-147	160
Trp-167	34
Trp-188	30
Trp-198	375
IIC^{mtl}-TL	358
Trp-97	2230

[a] Detergent-solubilized membrane vesicles; the errors in K_D are typically below 10% (21).

mission window of 405–445 nm (WG405, Lot-Oriel, Milan, Italy; plus interference filter DT-Blau, Balzer, Milan, Italy). The photomultiplier (EMI 9235QA, Middlesex, UK) was protected against fatigue from the strong excitation/fluorescence pulse by a mechanical chopper synchronized to the laser trigger, which closed the emission slit during the excitation pulse. The time resolution of this apparatus depends on the chopper speed and for the experiments reported here was maintained constant to 35 μs, the same as for spectral acquisitions. The photocurrent was amplified by a current-to-voltage converter (SR570, Stanford Research Systems, Stanford, CA) and digitized by a computerscope system (ISC-16, RC Electronics, Santa Barbara, CA) capable of averaging multiple sweeps. Typically, less than 100 sweeps was sufficient even for the shortest decays. The background emission, as determined by measurements carried out on a TL protein and on the surfactant-containing buffer, made an important contribution during the first 200–250 μs. Therefore, phosphorescence lifetimes shorter than 200 μs could not be determined accurately, and only the amplitudes of these short components could be estimated from the fluorescence-normalized phosphorescence intensities (24). To this end, parallel measurements were made of the intensity of prompt fluorescence from each excitation pulse. Prompt fluorescence was collected through a 310–375 bandpass filter combination (WG305 nm plus Schott UG11) and detected by a UV-enhanced photodiode (OSD100-7, Centronics, Newbury Park, CA). An analogue circuit was used to integrate the photocurrent, and its output was digitized and averaged by a multifunctional board (PCI-20428, Intelligent Instrumentation, Tucson, Texas) utilizing Lab View software. The prompt fluorescence intensity was used to account for possible variations in the laser output between phosphorescence and background measurements as well as to obtain fluorescence-normalized phosphorescence intensities. All phosphorescence decays were analyzed in terms of a sum of exponential components by a non-linear least squares fitting algorithm (Global Unlimited, LFD, University of Illinois).

RESULTS

Catalytic Properties of Single-Trp Mutants

The Trp-less and single-Trp EII and IIC mutants were tested for mannitol binding, and the results are summarized in TABLE ONE. All mutants bound mannitol with high affinity in the nanomolar range, comparable to the wild-type protein (21), except Trp-198 (K_D of 375 nM), Trp-97, and IIC-Trp-97, which showed a significant decreased binding affinity with K_D values of ~2 μM. The phosphorylation activities in intact membrane vesicles were more or less the same for all EII mutants and comparable to wild-type and TL (12), indicating the functionality of all mutants. Phosphorylation activity for the IIC mutants could not be measured, because they lack the IIBA^{mtl}-domains for phosphoryl-group transfer.

Fluorescence and Phosphorescence Characteristics of Single-Trp Mutants

For all mutants we have determined (i) the fluorescence spectrum in buffer at room temperature, (ii) the high resolution phosphorescence spectrum in a propylene glycol/buffer glass at 140 K, and (iii) the phosphorescence spectrum together with (iv) the phosphorescence decay in buffer at 273 K. Except for the glass-state measurements at 140 K (see "Materials and Methods"), the low background contribution of the TL proteins (both for EII and IIC) was not significantly different from that of the buffer and allowed us to correct the signals for the generally small contribution of the background. These observations were similar as made previously (14).

Fluorescence Spectra at Room Temperature—The fluorescence emission maximum (λ_F) provides an estimate of the polarity of the Trp environment as λ_F for the free chromophore increases from 300 nm in non-polar butanol to 350 nm in aqueous solutions (25). Only the emission of Trp-97 and IIC-Trp-97 showed a blue-shifted maximum (λ_F = 318 nm). The other mutants displayed maxima of >325 nm. The emission maxima of Trp-97 and IIC-Trp-97 are similar to that of tryptophan in hexane (320 nm), suggesting a very hydrophobic, non-polar environment for these residues.

Phosphorescence Spectra in Glasses at 140 K—In a rigid medium, as a low temperature glass, the spectrum of Trp displays a pronounced vibronic structure with a well resolved 0,0-vibrational band. Although the wavelength of the 0,0-vibrational band, $\lambda_{0,0}$, is related to the polarity-polarizability of the indole environment (26), its bandwidth (BW, the width at two-thirds height) reports on the structural homogeneity of the site (27). For free Trp in homogeneous solutions, $\lambda_{0,0}$ ranges from 406 nm for a polar aqueous solution, to 411 nm for a completely non-polar hydrocarbon solvent (26). In proteins, $\lambda_{0,0}$ ranges from 403 to 420 nm (27). In micellar solutions, as for detergent-solubilized EII or IIC, the solvent can be either aqueous or non-polar, depending on whether a particular region of the protein surface is solvated by water or by the lipid tails of the surfactant. Hence, only $\lambda_{0,0}$ values outside the range 406–411 nm imply effective burial of the indole within the folds of EII or IIC.

The highest spectral resolution is obtained with Trp residues buried in proteins having a unique conformation around the Trp site (*e.g.* Trp-72 of transhydrogenase from *Rhodospirillum rubrum*; BW = 3.2 nm) (28). Spectral broadening occurs on exposure of the aromatic ring to the solvent (BW = 5.7 nm for Trp in PG/water) and can be large (up to 15 nm), when the protein structure is not uniform at the Trp site, either because of local disorder or due to the presence of distinct conformers.

Examples of phosphorescence spectra at 140 K, showing the range of spectral resolutions, are given in Fig. 2*A* for mutants Trp-97 (well resolved) and Trp-147 (broad). The values of $\lambda_{0,0}$ and BW, derived from the phosphorescence spectra at 140 K, are reported for all mutants in TABLE TWO. According to the $\lambda_{0,0}$ values, only residue 97 is located in a polar site (406.7 nm). For the other mutants, $\lambda_{0,0}$ is between 409.0 and 411.7 nm, wavelengths compatible with predominantly non-polar environments. These findings indicate that in none of the mutant proteins the chromophore is exposed to the aqueous phase, either because the $\lambda_{0,0}$ is at a higher wavelength compared to Trp free in solution ($\lambda_{0,0}$ > 406 nm) or because in the case of Trp-97 it is much better resolved

(BW < 5.7 nm). We also note that for Trp-97, phosphorescence and fluorescence spectra apparently lead to opposite conclusions regarding the polarity of the Trp microenvironment, polar for the former, nonpolar for the latter. However, a blue-shifted fluorescence spectrum can also be indicative of a polar site that is too rigid to relax (shift to the red) during the fluorescence lifetime (26). The phosphorescence spectrum shows that for Trp-97 the latter interpretation is the correct one. A similar observation was made for Trp-72 in transhydrogenase from *R. rubrum* (28).

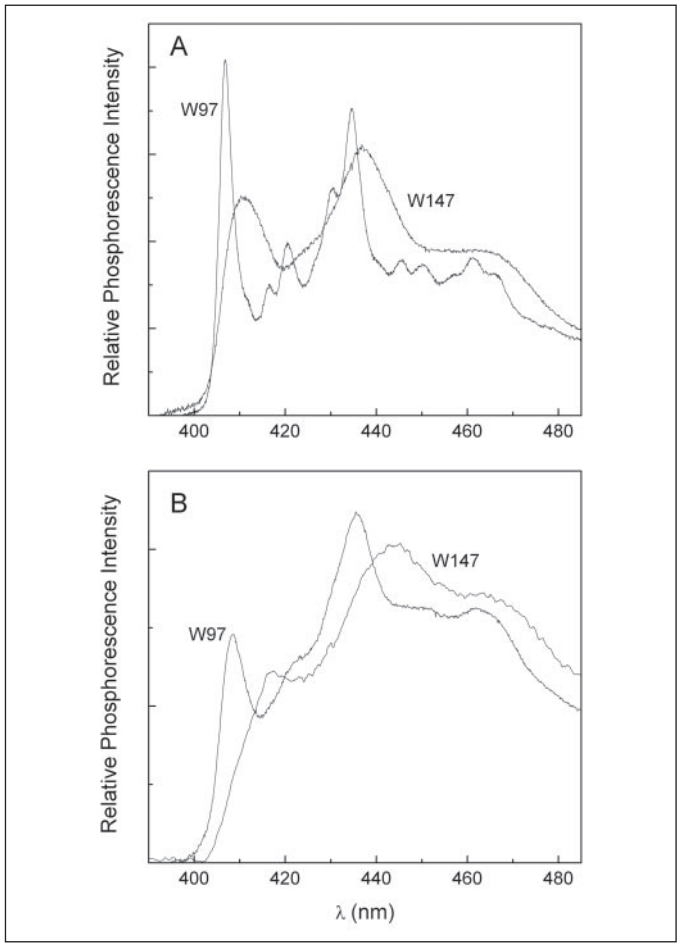

FIGURE 2. **High resolution phosphorescence spectra of Trp-97 and Trp-147 in PG/buffer glass at 140 K (*A*) and in buffer at 273 K (*B*).** Excitation wavelength λ_{ex} = 287 nm.

The BW of the 0,0-vibrational band is in most cases larger than for solvent-exposed Trp (BW = 5.7 nm). The lower spectral resolution in these mutants indicates multiple local configurations of the polypeptide and therefore structural heterogeneity. Exceptions are Trp-97, IIC-Trp-97 (BW = 3.4 nm), and Trp-114 (BW = 4.6 nm), which exhibit the best-resolved spectra. These sites are therefore rather homogeneous, implying an ordered local peptide structure. In the case of Trp-97, whose spectral resolution is among the highest ever reported for a globular protein fold, the spectrum is indicative of a unique, sharply defined structure around the chromophore, typical of tight β-sheet/barrel folds. Relative to Trp-97, the BW and local disorder increases progressively in the order Trp-114 < Trp-188 ~ Trp-66 ~ Trp-167 < Trp-198 ~ Trp-126 < Trp-133, to become large with Trp-147 (11.9 nm), suggesting a corresponding increase in conformational freedom at these sites.

Structural Flexibility from Thermal Spectral Relaxation in Buffer at 273 K—The gain in protein flexibility, as the temperature of glassy solutions is raised above the glass-transition state T_g (T_g ~ 200 K), allows the local structure to readjust itself around the triplet state dipole and achieve the lowest energy configuration. Thermal relaxation causes a red shift and broadening of the spectrum (10, 29). At near ambient temperature thermal population of near isoenergetic peptide conformations may also contribute to the loss in spectral resolution. As a rough guide, the larger the red shift and spectral broadening the more flexible and unstructured the protein site is. The average change in spectral energy (red shift) is generally indicated by the change in the center of gravity of the spectrum, $\Delta\lambda_g(T)$ [$\lambda_g = (\Sigma\lambda_i P_i)/(\Sigma P_i)$, with P_i the phosphorescence intensity at λ_i], a quantity that, unlike $\lambda_{0,0}$, takes into account the conformational heterogeneity.

Examples of spectral relaxations occurring in changing from the glass state at 140 K to liquid buffer at 273 K are shown in Fig. 2*B* for mutants Trp-97 and Trp-147. In either case the spectrum becomes red-shifted and broad, relative to the glass state. However, the spectrum of Trp-97 maintains a clear vibronic structure even after thermal relaxation, indicating that the environment at position 97 is ordered and rigid also in

TABLE TWO

Phosphorescence spectral energies and bandwidth of the 0,0-vibrational peak of the single-tryptophan mutants

All values are in nanometers; typical errors are $\lambda_{0,0}$, ±0.1 nm; BW, ±0.2 nm; λ_g, ±0.3 nm.

Mutant	$\lambda_{0,0}$[a]	BW[a]	λ_g^{LT}[b]	λ_g^{HT}[b]	$\Delta\lambda_g(T)$[c]	+1 mM mannitol[d]		
						$\Delta\lambda_{0,0}^{mtl}$[a]	ΔBW^{mtl}[a]	$\Delta\lambda_g^{mtl}$
	nm							
EII^{mtl}-Trp-66	411.7	6.8	442.0	447.1	+5.1	0	0	+2.7
Trp-97	406.5	3.4	436.8	441.3	+4.5	+2.3	+7.8	+3.3
Trp-114	409.0	4.6	439.3	445.3	+6.0	+0.6	0	+1.5
Trp-126	409.2	7.5	440.9	447.3	+6.4	+0.6	−0.2	0
Trp-133	409.9	8.5	440.1	446.6	+6.5	−0.5	−1.9	−0.8
Trp-147	410.2	11.9	441.3	449.6	+8.3	−0.9	−1.3	−1.8
Trp-167	409.0	6.8	439.3	448.4	+9.1	0	+0.6	+2.3
Trp-188	410.0	6.5	440.3	447.6	+7.3	0	+1.4	+0.1
Trp-198	410.0	7.4	440.3	447.1	+6.8	−0.9	0	+2.2
IIC^{mtl}-Trp-97	406.5	3.4	436.8	441.3	+4.5	+2.3	+7.8	+3.3

[a] Values refer to the phosphorescence spectra in glasses (T = 140 K).
[b] Center of gravity of the phosphorescence spectra, calculated according to $\lambda_g = (\Sigma\lambda_i P_i)/(\Sigma P_i)$; P_i is the phosphorescence intensity at λ_i; LT refers to measurements conducted at 140 K, HT refers to 273 K.
[c] $\Delta\lambda_g(T) = \lambda_g^{HT} - \lambda_g^{LT}$.
[d] Values refer to the shifts induced by the addition of 1 mM mannitol; $\Delta\lambda_g^{mtl} = \lambda_g$ (273 K) − λ_g^{mtl}(273 K).

fluid solutions. On the contrary, upon thermal relaxation the spectrum of Trp-147 became considerably more red-shifted and broad; the loss of resolution reduced the 0,0-vibronic band into a mere shoulder. Thus, this region of EII^{mtl} is relatively flexible, free to sample a variety of local structures.

The magnitude of the spectral shift, $\Delta\lambda_g(T)$, for the different mutants is given in TABLE TWO. The parameter $\Delta\lambda_g(T)$ is not simply correlated to the local flexibility of the environment as, other things being equal, it depends on the blue or red nature of the low temperature (starting) spectrum. That is because the maximum red shift of a high energy site (blue low temperature spectrum) is greater than that of a low energy site. When the starting spectral energy is taken into account, by decreasing/increasing the shift depending on whether λ_g (140 K) is to the blue/red of a reference state, we find that $\Delta\lambda_g$ (corrected) increases in the order Trp-97 < Trp-114 < Trp-126 < Trp-133 < Trp-66 ~ Trp-198 < Trp-188 < Trp-167 < Trp-147, which should reflect the ranking in local fluidity of the matrix around the indole group.

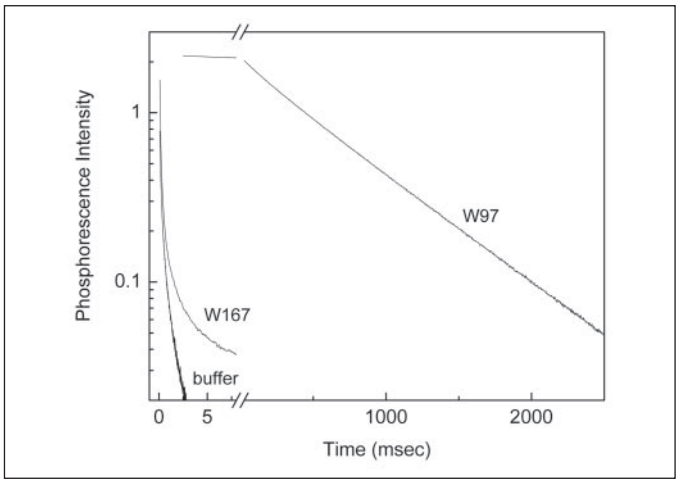

FIGURE 3. **Pulsed phosphorescence decays of Trp-97 and Trp-167 mutants in buffer at 273 K, together with the background signal of the buffer.**

Structural Fluidity and Homogeneity as Derived from the Phosphorescence Lifetime, τ, in Buffer at 273 K—Another sensitive parameter of the local protein/solvent mobility is the intrinsic phosphorescence lifetime, which decreases from about 6 s in rigid matrices to (sub) milliseconds in fluid solutions (11). Time-resolved measurements provide also information on the structural homogeneity of the protein site, as stable states of the protein ensemble differing in local flexibility will exhibit distinct lifetimes resulting in multiexponential phosphorescence decays.

The phosphorescence decays of Trp-97 and Trp-167 in buffer at 273 K are shown in Fig. 3 as extreme examples of decay kinetics among the various mutants. The decay of Trp-97 was the slowest and most uniform of all mutants, with an average lifetime (τ_{av}) of 576 ms. This is over 1000-fold longer than τ of Trp exposed to the solvent (the lifetime of *N*-acetyl-L-tryptophanamide in the same medium) and is characteristic of Trp residues buried in ordered, rigid cores of the polypeptide normally rich in β secondary structure. On the contrary, the phosphorescence emission of Trp-167 was very short-lived and heterogeneous, with most of the intensity decaying with sub-millisecond lifetimes. Because the detergent gave a strong background signal during the first 200 μs (Fig. 3, buffer), the lifetime of shorter-lived components could not be determined with accuracy. The results, however, do emphasize that Trp-167 is in a very fluid site, possibly through contact with the non-polar tails of the surfactant, and that its emission is effectively quenched by collision with reactive side chains and/or quenching impurities in the solvent.

The decay was heterogeneous with every mutant, showing that each protein site probed by Trp adopts multiple local conformations in the micellar medium. The lifetime components, τ_i, and corresponding ampli-

TABLE THREE

Lifetimes and amplitudes of the phosphorescence decay

Mutant	τ_1 [a]	α_1	τ_2	α_2	τ_3	α_3	τ_{av} [b]
	ms	*%*	*ms*	*%*	*ms*	*%*	*ms*
EII^{mtl}-Trp-66	<0.2	74	0.33	22	8.4	4	0.41–0.56
+mtl	<0.2	85	0.37	13	5.2	2	0.15–0.32
Trp-97			102	29	790	71	576
+mtl	1.49	42	8.1	56	64	2	6.4
Trp-114	<0.2	20	1.05	41	2.6	39	1.40–1.44
+mtl			0.37	58	2.38	42	1.21
Trp-126	<0.2	74	10	5	47	21	10.85–11.0
+mtl	1.79	35	10	44	52	21	15.9
Trp-133	<0.2	60	0.47	21	4.96	19	1.05–1.16
+mtl			0.81	19	7.15	81	5.89
Trp-147	1.78	80	8.7	17	52	3	4.67
+mtl	1.97	80	10	16	56	4	5.53
Trp-167	<0.2	82	0.30	16	2.93	2	0.11–0.28
+mtl	<0.2	90	0.36	8	3.14	2	0.09–0.26
Trp-188	<0.2	75	1.1	18	5.75	6.8	0.59–0.74
+mtl	<0.2	75	0.64	20	8.5	5	0.58–0.73
Trp-198	<0.2	10	1.52	64	6.6	26	2.7
+mtl	<0.2	40	1.67	44	8.5	16	2.1–2.2
IIC^{mtl}-Trp-97			130	12	630	88	570
+mtl	1.79	40	9.8	53	14	7	6.2

[a] Lifetime decays, τ_i, and corresponding amplitudes, α_i, from 2–3 exponential component fitting of the phosphorescence decay.
[b] Because of the strong background emission during the initial 200 μs, lifetimes shorter than this value could not be determined with accuracy. In these cases, the range in average lifetime, $\tau_{av} = \Sigma\alpha_i\tau_i$, is given, considering τ_1 either equal to 0 or to 0.2 ms. Errors in τ_{av} values between repeated measurements are ≤10%.

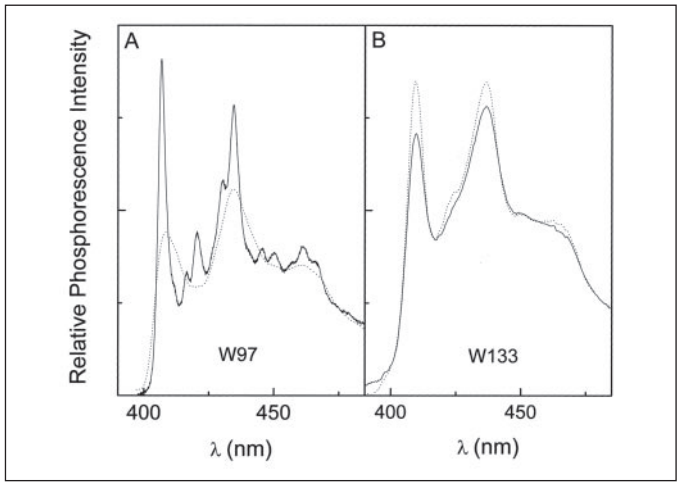

FIGURE 4. **Phosphorescence spectra of Trp-97 and Trp-133 in PG/buffer glass at 140 K, without (*solid*) and with (*dotted*) 1 mM mannitol.**

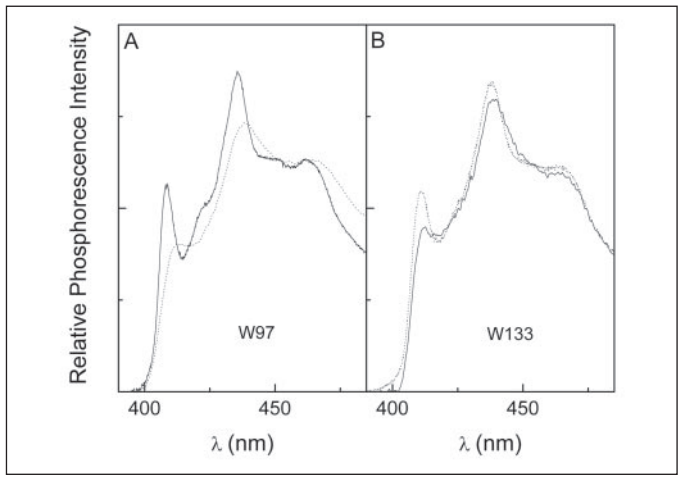

FIGURE 5. **Phosphorescence spectra of Trp-97 and Trp-133 in buffer at 273 K, without (*solid*) and with (*dotted*) 1 mM mannitol.**

tudes, α_i, derived from a discrete exponential fitting of the phosphorescence decay are collected in TABLE THREE. The table also reports the average lifetime, $\tau_{av} = \Sigma\tau_i\alpha_i$, or the range in τ_{av} when the initial part of the emission is overlapped by the background signal. Among the various mutants, τ_{av} ranks in the order Trp-97 ≫ Trp-126 > Trp-147 > Trp-198 > Trp-114 > Trp-133 > Trp-188 > Trp-66 > Trp-167. The lifetime of Trp-97 is characteristic for a Trp in a compact rigid core, whereas those of Trp-126, Trp-147, Trp-198, Trp-114, and Trp-133 are characteristic for residues buried within more or less flexible peptide folds, largely shielded from the solvent. The lifetime of the remainder Trp-188, Trp-66, and Trp-167 places the probe in superficial loose sites which, based on the non-polar nature of the environment, are probably in contact with the hydrophobic tails of the surfactant.

Effect of Mannitol Binding on the Fluorescence and Phosphorescence Emission

Mannitol binding changes the fluorescence and phosphorescence characteristics of some mutants considerably (Trp-97 and IIC-Trp-97), but leaves practically unaltered that of others (Trp-188). The change in fluorescent emission intensities was for most mutants <5% (data not shown), together with shifts of the maxima of <2 nm. The exceptions are Trp-66 with an 11% decrease in intensity and for the Trp at position 97 (Trp-97 and IIC-Trp-97) with 46% decrease in intensity together with a considerable red shift of 4 nm. According to the phosphorescent properties of the mutants, mannitol binding to the IIC^{mtl}-domain changes the polypeptide structure only in selected regions, some of which become more ordered and rigid (Trp-133 and Trp-147), whereas others become looser or more unfolded (Trp-66 and Trp-97). Examples of these opposite behaviors are provided by the phosphorescence properties of Trp-97 and Trp-133, as shown by the spectra in the glass-state at 140 K (Fig. 4), the spectra in buffer at 273 K (Fig. 5), and the phosphorescence lifetime in buffer at 273 K (Fig. 6).

From the low temperature spectrum, local changes in the polarity of the Trp environment can be inferred from the shift in $\lambda_{0,0}$ ($\Delta\lambda_{0,0}^{mtl}$), whereas variations in the degree of structural uniformity can be deduced from the change in bandwidth of the 0,0 band (ΔBW^{mtl}). For Trp-133 a slight blue shift ($\Delta\lambda_{0,0}^{mtl} = -0.5$ nm) of the spectrum was observed, together with a substantial increase in spectral resolution ($\Delta BW^{mtl} = -1.9$ nm), indicative of a structuring effect in that region upon mannitol binding (Fig. 4*B*). The effect was opposite and more dramatic for Trp-97 (Fig. 4*A*). The spectrum showed a pronounced red

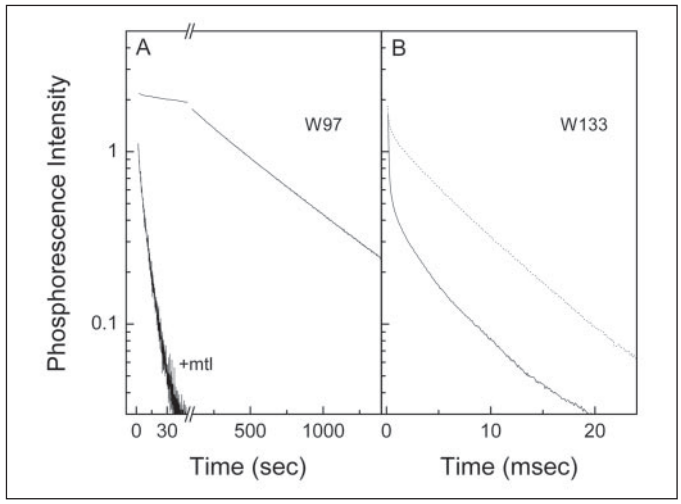

FIGURE 6. **Pulsed phosphorescence decays of Trp-97 and Trp-133 mutants in buffer at 273 K, without (*solid*) and with (*dotted*) 1 mM mannitol.**

shift ($\Delta\lambda_{0,0}^{mtl} = +2.3$ nm), implying a substantial change in composition of the groups surrounding the aromatic ring, which remains shielded from the aqueous phase. Furthermore, the extensive broadening of the spectrum ($\Delta BW^{mtl} = +7.8$ nm) is indicative of a multiplicity of different environments, and therefore loss of any organized structure. The magnitudes of both $\Delta\lambda_{0,0}^{mtl}$ and ΔBW^{mtl} for all mutants are reported in TABLE TWO. Based on these parameters a sharpening of the structure is reported for the Trps in Trp-126, Trp-133, and Trp-147, whereas unfolding is observed for Trp-97, Trp-167, and Trp-188. A slight change in the environment ($\Delta\lambda_{0,0}^{mtl}$), without affecting structural uniformity, is also found in the region of Trp-114 and Trp-198.

The effect of mannitol binding on the thermal relaxation of the spectrum and on the phosphorescence lifetime for mutants Trp-97 and Trp-133 is shown in Figs. 4–6. The differences in $\Delta\lambda_g^{mtl}$ and $\Delta\tau_{av}^{mtl}$ report on the influence of mannitol binding on the local flexibility of the various sites of the IIC-domain. For Trp-133 the spectrum in buffer becomes sharper and blue-shifted ($\Delta\lambda_g^{mtl} = -0.8$ nm). This implies that the surrounding polypeptide structure becomes more ordered, in full accord with a better-resolved low temperature spectrum. The phosphorescence decay of Trp-133 becomes more uniform, and the average lifetime increased by ~6-fold (Fig. 6 and TABLE THREE), confirming

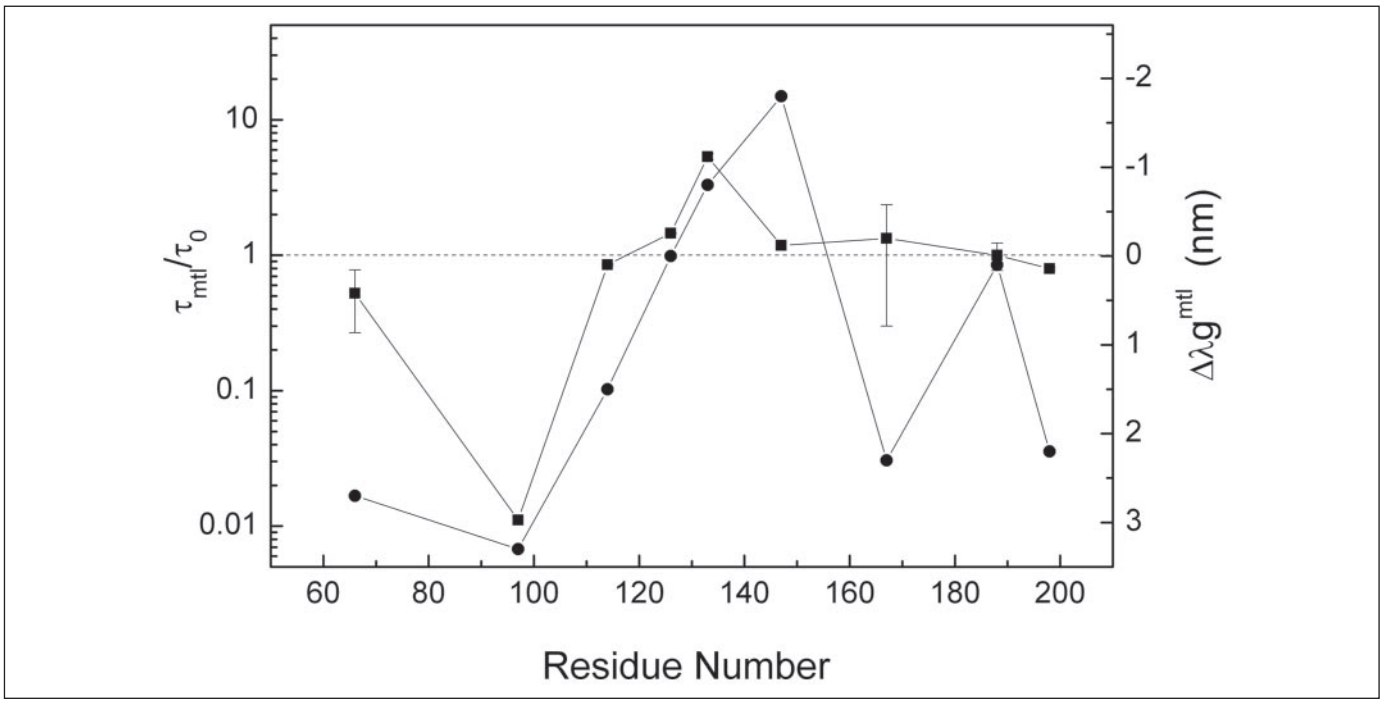

FIGURE 7. **Effects of mannitol binding on the flexibility of the IIC^{mtl}-domain at various positions.** The change in flexibility induced by mannitol binding is expressed as the ratio of the average lifetime with and without mannitol (τ_{mtl}/τ_0 (■)) and as the difference in the center of gravity, $\Delta\lambda_g^{mtl}$ (●), of the phosphorescence spectra of the mutants with and without mannitol at 273 K. *Error bars* indicate the range of the ratios of the lifetime values, reported in TABLE THREE.

an increased structural uniformity and rigidity when mannitol is bound. For Trp-97, binding of mannitol enhanced thermal relaxation of the spectrum ($\Delta\lambda_g^{mtl} = +2.4$ nm), which became broad and little resolved. The increase in flexibility was even more evident from the drastic almost 100-fold shortening of the phosphorescence lifetime, τ_{av} decreasing from 576 to 6.4 ms. According to the lifetime, the tight rigid core enveloping Trp-97 is lost in the mannitol-bound complex, suggesting that the process involves extensive unfolding of the local secondary structure. The spectral alteration induced by mannitol binding permitted us to attribute the shorting of the lifetime to a drastic increase in flexibility, rather than to potential intramolecular quenching reactions by cysteine, histidine, or tyrosine, triggered by the conformational change.

The results obtained with other mutants are summarized in TABLES TWO and THREE. For visual inspection, the changes induced by binding of mannitol on λ_g and on τ_{av} are also displayed in Fig. 7. The two flexibility parameters are well correlated and report roughly the same trend on the structural influence of mannitol in various sites of the IIC-domain. Thus, a structuring effect is reported in the region of Trp-133 and Trp-147 by $\Delta\lambda_g^{mtl}$, in the region of Trp-126, Trp-133, and Trp-147 by $\Delta\tau_{av}^{mtl}$. The structure became looser in the region of Trp-66, Trp-97, Trp-114, Trp-167, and Trp-198 on the basis of both $\Delta\lambda_g^{mtl}$ and $\Delta\tau_{av}^{mtl}$. No change in the spectrum or lifetime was observed for Trp-188.

DISCUSSION

Experimental knowledge about the dynamics of membrane-bound transport proteins during their catalytic cycle is scarce and limits the elucidation of the transport mechanism, including transporters of which the three-dimensional structure has recently been solved. The high sensitivity of tryptophan phosphorescence spectroscopy makes this an excellent tool to investigate membrane protein dynamics and heterogeneity.

In this investigation, we have characterized ten single-tryptophan mutants of the mannitol transporter (EII^{mtl}) from *E. coli*, both in a mannitol-bound and unbound state. The Trp positions were chosen to probe various structural elements of the membrane-embedded IIC^{mtl}-domain (Fig. 1). We showed previously that phosphorescence spectroscopy is suitable for studying membrane proteins, provided that the protein samples are pure, oxygen removal is efficient, and the detergent does not introduce quenching components and has a low background luminescence (14). Our data show that the microenvironments of the studied Trp positions vary from exposed and flexible sites to a very rigid protein matrix and that mannitol binding induces large conformational changes in the IIC^{mtl}-domain at several of these positions.

For all mutants, except Trp-97 and IIC-Trp-97, the Trps are in non-polar environments, shielded from the aqueous phase. The non-polar nature of Trp-66, Trp-167, and Trp-188, and their high flexibility could be indicative for exposed positions in contact with the hydrophobic tails of the detergent belt that surrounds the IIC^{mtl}-domain. Residues 66 and 167 are predicted in helices II and IV, respectively (Fig. 1). Taking their spectral characteristics into account these residues are therefore probably in contact with the hydrophobic core of the lipid bilayer.

In Fig. 7 the changes in microviscosity of the different residue positions induced by binding of mannitol are summarized. Until this study, changes in flexibility were expressed as the ratio of lifetimes with and without bound ligand (*e.g.* τ_{mtl}/τ_0). Implementation of a sensitive charge-coupled device camera in the experimental setup made it possible to estimate the changes in emission spectra in the glass and fluid state, upon mannitol binding ($\Delta\lambda_g^{mtl}$), in a routine fashion. An advantage of this parameter, compared with τ_{mtl}/τ_0, is that the latter can be biased by nearby quenching groups, challenging the relation between τ_p and local flexibility. Interestingly, our data show that in the case of mannitol binding both the τ_{mtl}/τ_0 and $\Delta\lambda_g^{mtl}$ parameters correlate very well (Fig. 7). Earlier, it was observed that the microenvironments of Trp-30 and (to a lesser extent) of Trp-42 changed upon mannitol binding (14). Taken together, mannitol binding induces significant conformational changes at most of the studied Trp positions in the IIC^{mtl}-domain, ranging from Trp-30 to Trp-198.

During the catalytic cycle of EII^{mtl}, an interaction is established between the IIB^{mtl}- and IIC^{mtl}-domains (1). A calorimetry study showed that, upon mannitol binding 50–60 residues become shielded from the aqueous phase (30). Because the effect was not observed for the IIC^{mtl} mutant (lacking IIBA^{mtl}), the data were interpreted as a docking of the IIB^{mtl}-domain onto the IIC^{mtl}-domain. Except for Trp-97, the involvement of the IIBA^{mtl}-domains on the phosphorescent properties of EII^{mtl} upon mannitol binding have not been investigated. The similarity of the phosphorescence data between Trp-97 and IIC-Trp-97, however, shows that large conformational changes occur in the IIC^{mtl}-domain in the absence of the IIBA^{mtl}-domains. Binding of mannitol results in loss of structure in mutants Trp-66, Trp-97, Trp-114, Trp-167, and Trp-198, and the microenvironment of the Trp becomes more structured in Trp-126, Trp-133, and Trp-147. A chemical cross-linking study showed that a cysteine at position 124 can form a disulfide bridge with Cys-384 in the IIB^{mtl}-domain (31). Possibly, the structuring observed for Trp-126, Trp-133, and Trp-147 upon binding of mannitol is a result of mannitol-induced interdomain interactions.

The most remarkable phosphorescence properties were observed for the tryptophan at position 97: a highly resolved phosphorescence spectrum both in the glass state at 140 K and in the fluid state at 273 K, together with a uniform and long phosphorescent lifetime. In fact, the spectrum of Trp-97 in buffer at 273 K (Fig. 2*B*) is one of the best-resolved spectra ever reported. Tryptophan phosphorescence lifetimes in the sub-second to second range are not common for proteins in fluid media and have only been observed for proteins with tryptophan residues in well defined, rigid protein cores, invariably formed by β-sheets/barrels. Examples are: Trp-48 of azurin ($\tau = 0.63$ s) (32), Trp-314 of horse liver alcohol dehydrogenase ($\tau_{av} = 0.65$ s) (33), Trp-109 of alkaline phosphatase from *E. coli* ($\tau = 2$ s) (33), and Trp-72 of the NAD(H)-binding component (dI) of *R. rubrum* transhydrogenase ($\tau = 2.9$ s) (28). Thus, the phosphorescence properties of the tryptophan in mutant Trp-97 strongly suggest that it is embedded in a β-sheet structure. Prediction of β-strands is in general difficult for (membrane) proteins. Although accurate estimation of the amount of β-sheet structures in the IIC^{mtl}-domain was not possible by Fourier transform IR analysis, a strong signal in the region of 1630–1634 cm^{-1} suggests that the protein contains a considerable fraction of β-sheet structure (34). The fact that the emission properties are identical both for Trp-97 and IIC-Trp-97 indicates that at least one β-sheet like core is located in the IIC^{mtl}-domain. Binding of mannitol induces a drastic change in the environment of Trp-97, indicative of local unfolding of the protein. Such a large effect of substrate binding on the phosphorescence spectrum and on the lifetime has not been reported before.

EII^{mtl} forms stable dimers both in the native membrane and in the detergent solubilized state, *i.e.* when solubilized by a polyethylene glycol-based detergent like $C_{10}E_5$ (18, 35–39). The high resolution of the spectrum of Trp-97 without mannitol suggests that both Trp residues in the dimer of Trp-97 are in a similar microenvironment. The large difference in lifetime between free and mannitol-bound Trp-97 indicate that mannitol binding influences both Trp residues in the dimer of Trp-97 in a similar manner when mannitol interacts at the single binding site present in the dimer (20).

Currently, no information is available where sugar translocation takes place in EII^{mtl} or the other sugar translocators belonging to the phosphoenolpyruvate-dependent phosphotransferase system (PTS) family. The data presented in this report show for the first time that a significant part of the sugar translocation domain undergoes structural changes, including unfolding of a rigid protein core around residue position 97. The large impact of the Phe-97 to Trp mutation on the mtl binding affinity suggests that it is located close to the mannitol binding site. The localization of the studied tryptophan residues with respect to the mannitol binding site is currently investigated via fluorescence resonance energy transfer experiments using a chromophoric analogue of mannitol (15).

REFERENCES

1. Robillard, G. T., and Broos, J. (1999) *Biochem. Biophys. Acta* **1422,** 73–104
2. Grisafi, P. L., Scholle, A., Sugiyama, J., Briggs, C., Jacobson, G. R., and Lengeler, J. W. (1989) *J. Bacteriol.* **171,** 2719–2727
3. Elferink, M. G. L., Driessen, A. J. M., and Robillard, G. T. (1990) *J. Bacteriol.* **172,** 7119–7125
4. Lolkema, J. S., Swaving-Dijkstra, D., Ten Hoeve-Duurkens, R. H., and Robillard, G. T. (1990) *Biochemistry* **29,** 10659–10663
5. Lolkema, J. S., Ten Hoeve-Duurkens, R. H., Swaving-Dijkstra, D., and Robillard, G. T. (1991) *Biochemistry* **30,** 6716–6721
6. Sugiyama, J. E., Mahmoodian, S., and Jacobson, G. R. (1991) *Proc. Natl. Acad. Sci. U. S. A.* **88,** 9603–9607
7. Lengeler, J. W., Jahrkreis, K., and Wehmeier, U. F. (1994) *Biochim. Biophys. Acta* **1188,** 1–28
8. Vervoort, E. B., Bultema, J. B., Schuurman-Wolters, G. K., Geertsma, E. R., Broos, J., and Poolman, B. (2005) *J. Mol. Biol.* **346,** 733–743
9. Koning, R. I., Keegstra, W., Oostergetel, G. T., Schuurman-Wolters, G. K., Robillard, G. T., and Brisson, A. (1995) *J. Mol. Biol.* **287,** 845–851
10. Strambini, G. B., and Gonnelli, M. (1995) *J. Am. Chem. Soc.* **117,** 7646–7651
11. Gonnelli, M., and Strambini, G. B. (2005) *Photochem. Photobiol.* **81,** 614–622
12. Swaving-Dijkstra, D., Broos, J., Lolkema, J. S., Enequist, H., Minke, W., and Robillard, G. T. (1996) *Biochemistry* **35,** 6628–6634
13. Swaving-Dijkstra, D., Broos, J., Visser, A. J. W. G., Van Hoek, A., and Robillard, G. T. (1997) *Biochemistry* **36,** 4860–4866
14. Broos, J., Strambini, G. B., Gonnelli, M., Vos, E. P. P., Koolhof, M., and Robillard, G. T. (2000) *Biochemistry* **39,** 10877–10883
15. Broos, J., Pas, H. H., and Robillard, G. T. (2002) *J. Am. Chem. Soc.* **124,** 6812–6813
16. Broos, J., Maddalena, F., and Hesp, B. (2004) *J. Am. Chem. Soc.* **126,** 22–23
17. Meijberg, W., Schuurman-Wolters, G. K., Boer, H., Scheek, R. M., and Robillard, G. T. (1998) *J. Biol. Chem.* **273,** 20785–20794
18. Boer, H., Ten Hoeve-Duurkens, R. H., Schuurman-Wolters, G. K., Dijkstra, A., and Robillard, G. T. (1994) *J. Biol. Chem.* **269,** 17863–17871
19. Broos, J., Ter Veld, F., and Robillard, G. T. (1999) *Biochemistry* **38,** 9798–9803
20. Veldhuis, G., Broos, J., Poolman, B., and Scheek, R. M. (2005) *Biophys. J.* **89,** 201–210
21. Veldhuis, G., Vos, E. P. P., Broos, J., Poolman, B., and Scheek, R. M. (2004) *Biophys. J.* **86,** 1959–1968
22. Robillard, G. T., and Blaauw, M. (1987) *Biochemistry* **26,** 5796–5803
23. Swaving-Dijkstra, D., Broos, J., and Robillard, G. T. (1996) *Anal. Biochem.* **240,** 142–147
24. Strambini, G. B., Kerwin, A. B., Mason, D. B., and Gonnelli, M. (2004) *Photochem. Photobiol.* **80,** 462–470
25. Konev, S. V. (1967) *Fluorescence and Phosphorescence of Proteins and Nucleic Acids*, Plenum Press, NY
26. Galley, W. C. (1976) in *Concepts of Biochemical Fluorescence* (Chen, R. F. and Edelhoch, H., eds) Vol. 2, Chap. 8, pp. 409–439, Marcel Dekker, New York
27. Herschberger, M. V., Maki, A. H., and Galley, W. C. (1980) *Biochemistry* **19,** 2204–2209
28. Broos, J., Gabellieri, E., Van Boxel, G. I., Jackson, J. B., and Strambini, G. B. (2003) *J. Biol. Chem.* **278,** 47578–47584
29. Strambini, G. B., and Gonnelli, M. (1985) *Chem. Phys. Lett.* **115,** 196–200
30. Meijberg, W., Schuurman-Wolters, G. K., and Robillard, G. T. (1998) *J. Biol. Chem.* **273,** 7949–7956
31. Van Montfort, B. A., Schuurman-Wolters, G. K., Duurkens, R. H., Mensen, R., Poolman, B., and Robillard, G. T. (2001) *J. Biol. Chem.* **276,** 12756–12763
32. Cioni, P., De Waal, E., Canters, G. W., and Strambini, G. B. (2004) *Biophys. J.* **86,** 1149–1159
33. Gonnelli, M., and Strambini, G. B. (1995) *Biochemistry* **34,** 13847–13857
34. Robillard, G. T, Boer, H., Haris, P. I., Meijberg, W., Swaving-Dijkstra, D., Schuurman-Wolters, G. K., Ten Hoeve-Duurkens, R., Chapman, D., and Broos, J. (1996) in *Handbook of Biological Physics* (Hoff, A. J., Series ed; Konings, W. N., Kaback, H. R., and Lolkema, J. S., Volume eds) Vol. 2, pp. 549–572, North-Holland, Elsevier
35. Khandekar, S. S., and Jacobson, G. R. (1989) *J. Cell. Biochem.* **39,** 207–216
36. Lolkema, J. S., Kuiper, H., Ten Hoeve-Duurkens, R. H., and Robillard, G. T. (1993) *Biochemistry* **32,** 1396–1400
37. Pas, H. H., Ellory, J. C., and Robillard, G. T. (1987) *Biochemistry* **26,** 6689–6696
38. Roossien, F. F., and Robillard, G. T. (1984) *Biochemistry* **23,** 5682–5685
39. Stephan, M. M., and Jacobson, G. R. (1986) *Biochemistry* **25,** 4046–4051
40. Sonnhammer, E. L., Von Heijne, G., and Krogh, A. (1998) *Proc. Int. Conf. Intell. Syst. Mol. Biol.* **6,** 175–182